Showcasing research from Professor Wang's laboratory, College of Chemistry, Nankai University, Tianjin 300071, China.

EDTA etching: a simple way for regulating the traps, size and aqueous-dispersibility of Cr^{3+}-doped zinc gallate

The traps, size and aqueous-dispersibility are the most important parameters that affect the features and applications of persistent luminescent nanoparticles (PLNPs). However, the simultaneous controlling of those parameters is rather difficult and has not been reported yet. We present the first exploration on adjusting the traps, size and aqueous-dispersibility of PLNPs via a simple ethylenediaminetetraacetate (EDTA) etching. The EDTA etching of the sintered $Cr^{3+}_{0.004}$:$ZnGa_2O_4$ results in effective reduction of the size, great improvement of the aqueous-dispersibility, but meanwhile altering the density of mediate traps and generating the new deep traps.

As featured in:

Chemical Science

ROYAL SOCIETY OF CHEMISTRY

rsc.li/chemical-science

Check for updates

EDTA etching: a simple way for regulating the traps, size and aqueous-dispersibility of Cr³⁺-doped zinc gallate†‡

He-Fang Wang, [ID] *[ab] Xi Chen,[a] Fan Feng,[a] Xia Ji[a] and Ye Zhang[a]

Traps, size and aqueous-dispersibility are the most important parameters that affect the features and applications of persistent luminescent nanoparticles (PLNPs). However, simultaneous controlling of these parameters is rather difficult and has not been reported yet. We present the first exploration on adjusting the traps, size and aqueous-dispersibility of PLNPs *via* simple ethylenediaminetetraacetate (EDTA) etching. $Cr_{0.004}^{3+}$:$ZnGa_2O_4$ (ZGO) was used as the PLNP model. EDTA etching of the sintered ZGO results in effective reduction of the size and great improvement in the aqueous-dispersibility. In addition, EDTA etching alters the density of mediate traps and generates new deep traps, thus achieving the massive production of (ultra)small ZGO–EDTA with fine aqueous-dispersibility, suitable mediate/deep traps and superlong bright afterglows (51 days). As EDTA can interact with most metals, this simple EDTA etching strategy is prospectively amenable to other PLNPs, and the resulting PLNPs–EDTA have wide applications in both biological field and information storage.

Introduction

Persistent luminescent nanoparticles (PLNPs)[1–5] have aroused considerable attention in pre-excitation optosensing,[6–10] bioimaging,[11–28] drug delivery,[29–31] imaging-guided therapy,[6,32–36] and information storage.[22,37–39] Traps, size and aqueous-dispersibility are the most important parameters that affect the features and applications of PLNPs. For instance, the density of mediate traps (0.5–0.8 eV) is considered to be inter-related with the room temperature (RT) afterglow intensity and durations. Deep traps of 0.8–1.6 eV are required for retaining the recorded information for long time,[37,38] while the size and aqueous-dispersibility of PLNPs are the key factors in biological applications.[40] Some studies have reported the low-temperature-synthesis methods, including the hydrothermal (200–220 °C[7,41,42]), biphasic (160 °C)[43] and microwave-assisted non-aqueous sol–gel (270 °C),[44] to obtain the small-sized PLNPs, but without controlling the traps. Others reported doping with different codopants for engineering the trap depth,[37,38] but with no ideas on adjusting the size and dispersibility. To the best of our knowledge, simultaneous

controlling of the traps, size and dispersibility of PLNPs is a formidable task, and has not been reported yet.

Herein, we present the first exploration on adjusting the traps, size and aqueous-dispersibility of PLNPs *via* a simple post-treatment of ethylenediaminetetraacetate (EDTA) etching. The widely reported $Cr_{0.004}^{3+}$:$ZnGa_2O_4$ (ZGO) was used as the PLNP model. The ZGO synthesized by the biphasic method[43] was sintered at 1000 °C and then treated with EDTA solutions at different temperatures, pH values and amounts (Scheme 1, the details are elaborated in ESI‡). EDTA etching prioritizes in dissolving the interparticle necks between the sintered ZGO nanoparticles, and thus breaks the large particles down into the small particles. Moreover, the EDTA etching drives some metals

[a]Research Center for Analytical Sciences, College of Chemistry, Nankai University, Tianjin Key Laboratory of Biosensing and Molecular Recognition, State Key Laboratory of Medicinal Chemical Biology, Tianjin 300071, China. E-mail: wanghefang@nankai.edu.cn

[b]Collaborative Innovation Center of Chemical Science and Engineering (Tianjin), Tianjin 300071, China

† This article is dedicated to the 100th anniversary of Nankai University.

‡ Electronic supplementary information (ESI) available. See DOI: 10.1039/c8sc04173c
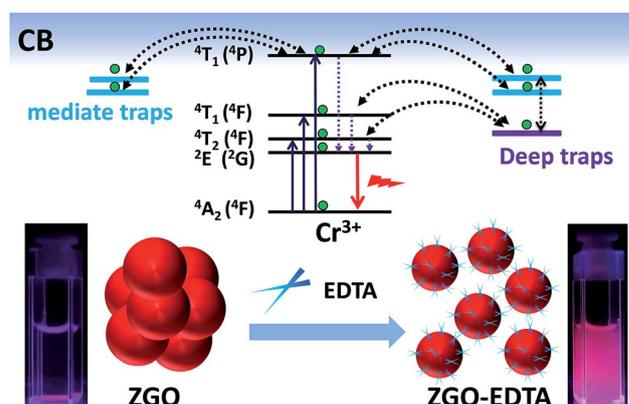
Scheme 1 The strategy of EDTA etching for regulating the traps, size and aqueous-dispersibility of ZGO.

in ZGO into the supernatants, resulting in further reduction of the size, and the departure of Ga and Zn takes away the linked oxygens and thus generates some oxygen vacancies (corresponding to deep traps) neighboring the remaining Ga and Zn on the resulting nanoparticles of ZGO–EDTA.

To demonstrate the hypothesis, we collected and analyzed the liquid supernatants after the EDTA-treatment by inductively coupled plasma-atomic emission spectroscopy (ICP-AES) to examine the etching amount of the metals. Moreover, the harvested solid particles were dried and evaluated in the aspects of the yield, size, aqueous-dispersibility, photoluminescence (PL), thermo-luminescence (TL) and afterglows. We show that EDTA etching can regulate the traps, size, and aqueous-dispersibility of the resultant ZGO–EDTA nanoparticles. We discuss the reason behind EDTA etching and applications of the ZGO–EDTA nanoparticles in *in vivo* bioimaging and information storage. To the best of our knowledge, EDTA etching is the first strategy that can simply generate the deep traps while reducing the size and improving the aqueous-dispersibility.

Results and discussion

EDTA etching

The treatments by EDTA solutions at different temperatures (RT and 220 °C), pH (4, 7, 10, 13) and amounts (1, 3, 5, 7 equivalent weight of ZGO) were examined. We first measured the contents of metals in the supernatants treated with EDTA under various conditions and with water, HNO_3-pH4, and NaOH-pH13 (the treatments are at 220 °C unless stated otherwise, Table S1‡ and Table 1, the corresponding percentages against the nominal amounts are also listed). The supernatants treated with water and HNO_3-pH4 have negligible contents of Ga, Zn and Cr, and the treatment with EDTA at RT (5EDTA-pH13-RT) results in a small quantity of Ga, Zn and Cr in the supernatant. On the contrary, the supernatants treated with 5EDTA-pH (4, 7, 10 and 13) and NaOH-pH13 own substantial concentrations and corresponding percentages of Ga and Zn. The highest and lowest erosion percentage of Ga and Zn are observed at 5EDTA-pH4 and 5EDTA-pH10, respectively. Compared with the data of HNO_3-pH4 and NaOH-pH13, the etching percentage of EDTA at

identical pH (4 or 13) is significantly high toward Ga and Zn. For Cr, the various amounts of EDTA solutions at pH 13 show the lowest etching percentage. Currently, the reason behind these erosion data is not well understood. One fact we can think of is that Ga, Zn and Cr are amphoteric; thus, ZGO can be partly etched by EDTA solutions at various pH. Among those treatments (Tables S1‡ and 1), EDTA solutions at pH 13 show substantial etching ability toward Ga and Zn (the matrix of ZGO), but very low erosion ability toward Cr, having the potential of reducing the size while maintaining the luminescent center. Thus, we systematically examined the etching cases of various amounts of EDTA at pH 13 in subsequent studies. We note that the etching percentage of Zn is lower than that of Ga (Table 1), resulting in the increase in Zn/(Ga + Cr) ratio of the resultant ZGO–nEDTA (n = 1, 3, 5, 7) nanoparticles, which leaves more chances for Cr^{3+} to neighbor the antisite defect and finally generate the more intense N_2 emission (695 nm) than R emission (688 nm) in PL spectra[45] (Fig. S1‡).

We then tested the harvested amounts of ZGO–nEDTA after etching. To imitate the selective sedimentation, all solids after corrosion were re-dispersed in ultrapure-water and settled for 10 min, and the solid in suspensions (marked as ZGO–nEDTA-S) and sediments (marked as ZGO–nEDTA-B) were collected (ZGO-S and ZGO-B are the products from tradition grinding, without hydrothermal treatment). Table S2‡ lists the amounts and the corresponding yields. The traditional grinding gives 4.7% of ZGO-S and 90% of ZGO-B. In contrast, the EDTA etching produces more solid in suspensions (ZGO–nEDTA-S) and less solid in sediments (ZGO–nEDTA-B). The decreased total amounts of ZGO–nEDTA (the sum of S and B) are ascribed to the corrosion by EDTA, as listed in Table 1. The yields of ZGO–nEDTA-S gradually increased with the increase in amount of EDTA, giving the highest yield of 40% when 5EDTA was used. Further increase in EDTA results in slightly lower yield of ZGO–7EDTA-S (35.1%) than ZGO–5EDTA-S (40%), but higher yield of ZGO–7EDTA-B (34.3%) over ZGO–5EDTA-B (23.3%). It is worth noting that the solid in suspensions should have smaller size and/or more water-dispersible ligands than that in sediments. The following section gives the explanation.

Table 1 The concentration (conc., mean ± SD) and the corresponding erosion percentage (P, mean ± SD) of the metals existing in the supernatants from hydrothermal treatment of ZGO with different amounts of EDTA at pH 13 and water

Entry	Ga		Zn		Cr	
	Conc.[a] (mg L^{-1})	P[b] (%)	Conc.[a] (mg L^{-1})	P[b] (%)	Conc.[a] (mg L^{-1})	P[b] (%)
1EDTA	1813 ± 38	35.0 ± 0.7	542 ± 41	22.3 ± 1.7	0.022 ± 0.004	0.22 ± 0.04
3EDTA	2125 ± 67	41.0 ± 1.3	712 ± 21	29.3 ± 0.9	0.015 ± 0.005	0.15 ± 0.05
5EDTA	2233 ± 143	43.1 ± 2.8	714 ± 42	29.4 ± 1.7	0.030 ± 0.016	0.30 ± 0.16
7EDTA	1713 ± 38	33.0 ± 0.7	441 ± 1	18.1 ± 0.03	0.020 ± 0.001	0.21 ± 0.01
H_2O	0.19 ± 0.04	<0.01	<0.005	<0.01	<0.004	<0.05

[a] The concentration of each metal is detected by ICP-AES. [b] The erosion percentage is calculated by $\dfrac{cV}{m \times \dfrac{nM_m}{M}} \times 100\%$, where c is the concentration of individual metal in the supernatant; V is the volume of the supernatant; m is the mass of raw ZGO; M_m is the molar mass of the individual metal; n is the number of the individual metal in nominal formula of ZGO; and M is the molar mass of ZGO calculated from the nominal formula.

Chemical Science
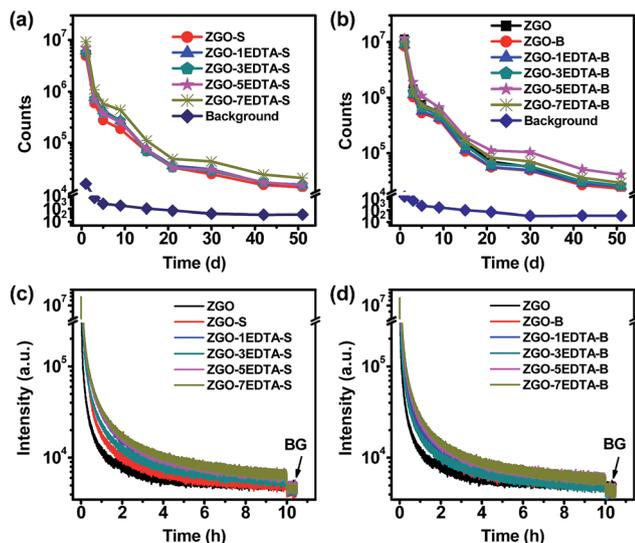
Fig. 3 The afterglow decays of (a) solid ZGO-S and ZGO–nEDTA-S, (b) solid ZGO, ZGO-B and ZGO–nEDTA-B, (c) aqueous dispersions of ZGO, ZGO-S and ZGO–nEDTA-S and (d) aqueous dispersions of ZGO, ZGO-B and ZGO–nEDTA-B (n =1, 3, 5, 7). For (a) and (b), 3 mg of solid was irradiated by a 254 nm UV lamp (6 W) for 5 min, and the afterglow images and intensity were recorded using a CCD camera at different durations after stoppage of irradiation. For (c) and (d), 3 mL of 2 g L^{-1} aqueous dispersions was pre-lighted by a 254 nm UV lamp for 5 min and then was put into the sample holder immediately for recording the afterglow at 695 nm using a PTI fluorescence spectrophotometer.

B over ZGO–5EDTA-RT-B during the first 30 days, while the deep traps of ZGO–5EDTA-RT-B result in the reverse on the 42nd day (Fig. S6d‡). All these data suggest that the mediate traps are related to the afterglow intensity at early durations. After depletion of the electrons in mediate traps, the electrons in deep traps can be released and retrapped by mediate traps, and generate the afterglows of the late stage (the electrons trapped in mediate traps are emptied faster than those in deep traps, as revealed by the decay time-dependent TL measurements in Fig. S8‡). It should be noted that the maintained or enhanced afterglows of the ZGO–nEDTA are companied with the reduced size, which is quite different from the reported PL enhancement of the hydrothermal treatments (where the particle size keeps invariable).

It is worth noting that the afterglow of all solid ZGO, ZGO-S, ZGO-B and ZGO–nEDTA is bright at the 51st day (Fig. S7‡), with the highest signal-to-noise ratio (SNR) of 115 (ZGO–5EDTA-B) and the lowest SNR of 38 (ZGO-S). The ZGO–nEDTA-S (n = 1, 3, 5, and 7) have smaller size than ZGO-S (Fig. 1a), but own higher afterglow than ZGO-S (Fig. 3a and S7‡). Similarly, ZGO–nEDTA-B (n = 1, 3, 5, and 7) also have smaller size (Fig. 1b) but higher afterglow (Fig. 3b) than ZGO-B. These data demonstrate the superiority of EDTA etching in maintaining or enhancing the afterglow when reducing the size. It should be noted that the ZGO–nEDTA-B (n = 3, 5, 7) even own higher afterglow intensity than the raw ZGO, which is the first case of reducing the size but increasing the afterglow of nanoparticles.

As many applications require using the aqueous dispersions, we measured the afterglow spectra (Fig. S1‡) and decays (Fig. 3c

and d) of the aqueous dispersions of ZGO–nEDTA, ZGO-S, ZGO-B and ZGO using a fluorometer. As shown in Fig. S1,‡ ZGO–nEDTA (n = 1, 3, 5, 7) displays higher intensity in both PL and afterglow spectra. Furthermore, smaller size, better aqueous-dispersibility, and higher intensity are observed. More significant difference is observed in the afterglow intensity because the difference in aqueous-dispersibility is magnified when the aqueous suspensions are settled for longer time in measurements of afterglow spectra. Similarly, the afterglow decays of the aqueous dispersions measured using a fluorometer are mainly related to aqueous-dispersibility and not only the traps. ZGO–nEDTA has much better aqueous-dispersibility. Thus, all the aqueous dispersions of the small-sized ZGO–nEDTA display higher afterglow intensity than that of the large-sized ZGO during the decays (Fig. 3c and d), which is quite different from the results of the measurements in solid form (Fig. 3a and b). For the same reason, the aqueous dispersions of the ZGO–nEDTA-S have higher afterglow intensity than the corresponding ZGO–nEDTA-B. For the aqueous dispersions of S or B series, the more the EDTA used, the higher the afterglow intensity observed in afterglow decays. This elucidates the regulation role of EDTA in adjusting the size, aqueous-dispersibility and afterglows of ZGO–nEDTA. It is worth noting that the afterglows of aqueous dispersions of ZGO–nEDTA are higher than the background (BG) at 10 h.

The erosion mechanism

The sintering process greatly enhances the afterglows, but with the price of converting the primary powder into the hard-agglomerated particles *via* the formation of interparticle necks with different curvature and crystallinity degree.[46] The erosion by EDTA prioritizes the dissolution of such interparticle necks between the agglomerated ZGO nanoparticles, and thus breaks the large particles down into the small ones. Moreover, EDTA etching drives some metals (mainly Ga and Zn) into the supernatants (Table 1 and S1‡), which results in further reduction of the size (Fig. 1), but without significant change in the spinel phase of ZnGa$_2$O$_4$ (JCPDS 38-1240, Fig. S9‡). As all Ga and Zn atoms were connected to several oxygen atoms, the departure of Ga and Zn inevitably takes away the linked oxygen atoms and thus generates some oxygen vacancies neighboring the remaining Ga and Zn sites on the resultant ZGO–nEDTA.

To verify the oxygen vacancies generated by EDTA erosion, we compared the XPS (Fig. 4) and ESR spectra (Fig. 5) of ZGO and the typical ZGO–5EDTA. The symmetric peaks of Ga 2p$_{3/2}$ (1117.5 eV) and Zn 2p$_{3/2}$ (1021.2 eV) of ZGO suggest that the Ga^{3+} ions are located at the octahedral sites and Zn^{2+} ions are located at the tetrahedral sites[47] (Fig. 4). The corresponding peaks of ZGO–5EDTA (both S and B) are still symmetric, but positively shift to around 1117.8 (Ga) and 1021.8 eV (Zn). Moreover, the O$_{1S}$ peak in ZGO is at 530.4 eV, but that in ZGO–5EDTA (both S and B) is observed at 531.0 eV. Similarly, the binding energy of Cr 2p$_{3/2}$ is also enlarged in ZGO–5EDTA. These positively shifted binding energies of Ga, Zn, Cr and O in ZGO–5EDTA are ascribed to the neighboring electron-attracting oxygen vacancies.[48] The extra tailing peaks at around 533 eV of
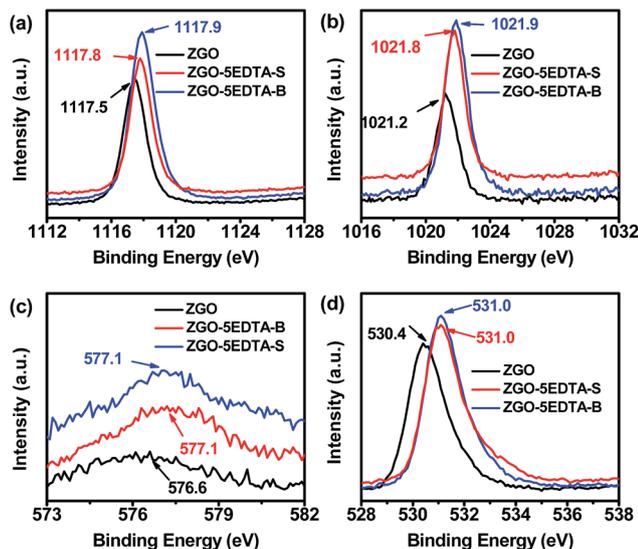
Fig. 4 XPS spectra of (a) Ga $2p_{3/2}$, (b) Zn $2p_{3/2}$, (c) Cr $2p_{3/2}$ and (d) O 1s of ZGO, ZGO–5EDTA-S and ZGO–5EDTA-B.
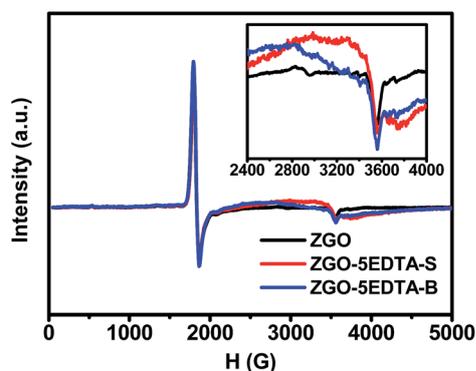

Fig. 5 ESR spectra of ZGO, ZGO–5EDTA-S and ZGO–5EDTA-B.

ZGO–5EDTA are ascribed to the oxygen of the attached EDTA, which is in accordance with the results of zeta potentials (Fig. 1) and FT-IR (Fig. S4‡). Further calculations of the surface atomic concentration from XPS spectra reveal that ZGO has the ratio of $Cr_{0.005}$:$Zn_{0.365}GaO_{2.00}$, while the atom ratios of ZGO–5EDTA-S and ZGO–5EDTA-B are $Cr_{0.006}$:$Zn_{0.438}GaO_{1.85}$ and $Cr_{0.006}$:$Zn_{0.428}GaO_{1.80}$, respectively. Compared with ZGO, the surface of ZGO–5EDTA has more Zn atoms (in according with Table 1), but less O atoms. All these XPS data prove that the ZGO–5EDTA nanoparticles (both B and S) have oxygen vacancies.

In ESR (Fig. 5), the signals near 3555 G ascribed to the Cr^{3+} ions in the undisturbed sites of $ZnGa_2O_4$ host[49] are both observed in ZGO and ZGO–5EDTA, but ZGO–5EDTA shows the extra conspicuous broad peaks in the range of 2400–4000 G (the g-factor of the peak at 3560 G is 1.9745), which identify the existence of oxygen vacancies.[50] These oxygen vacancies, related to the deep traps[51] in TL (Fig. 2), are responsible for the maintained or enhanced afterglow of ZGO–nEDTA with reduced size, as discussed above.

Application in afterglow imaging *in vivo*

We examined the *in vivo* afterglow imaging and the corresponding biodistribution of ZGO and ZGO–5EDTA in normal mice (Fig. S10‡) and MCF-7 tumor-bearing mice (Fig. 6). The afterglow images with high SNR of both ZGO and ZGO–5EDTA are clearly detected without any external illuminations within 6 h. At 24 h, the afterglow images with high SNR were observed with the help of *in vivo* activation using a 650 nm LED for 1 min. For normal mice, a great difference in the biodistribution of ZGO–5EDTA and ZGO (Fig. S10‡) is observed because ZGO displays much higher existence in the lung and the spleen, while the ZGO–5EDTA has slightly higher existence in the liver. For MCF-7 tumor-bearing mice, the SNRs in the liver of the mice injected with ZGO and ZGO–5EDTA are very similar (54 *vs.* 56) at 3 h. However, the SNR in tumor of the mice injected with ZGO–5EDTA (26) is higher than that of the mice injected with ZGO (15). With passage of time, ZGO–5EDTA displays gradual accumulation in the tumor and gradual elimination in the liver. For example, at 6 h, the SNR in the tumor is 35, whereas the SNR in the liver is 17. At 24 h (the mice were *in vivo* activated using a 650 nm LED for 1 min), the SNR in the tumor is 1174, but the SNR in the liver is only 23. The SNR of the tumor and the liver of the mice injected with ZGO–5EDTA gradually increased with time. In contrast, the mice injected with ZGO exhibited gradually decreased SNR ratio in the tumor and the liver (at 3, 6 and 24 h, the ratio is 15/54, 3.7/21 and 4.2/171, respectively). The biodistribution of ZGO and ZGO–5EDTA in the organs and tumor at 24 h (Fig. 6c and d) was in accordance with the *in vivo* images (Fig. 6a and b). The vital biodistribution difference between the mice injected with ZGO–5EDTA and ZGO is most probably ascribed to the much smaller size and much better aqueous dispersibility of ZGO–5EDTA than ZGO,[40] demonstrating the great superiority of ZGO–5EDTA in biological applications.
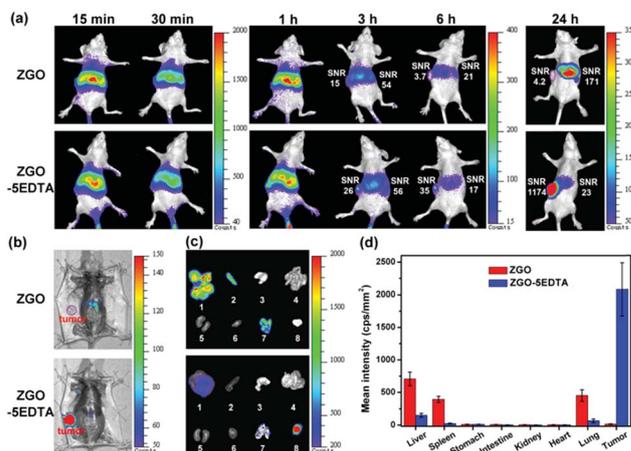
Fig. 6 (a) Afterglow images of MCF-7 tumor-bearing mice after intravenous injection of ZGO and ZGO–5EDTA (0.1 mg, 5 min of irradiation using a 254 nm UV lamp before injection). (b) NIR afterglow images of the mice at 24 h in panel (a), without the superficial skin. (c) Representative afterglow images of isolated organs from the mice in panel (a): (1) liver, (2) spleen, (3) stomach, (4) intestine, (5) kidney, (6) heart, (7) lung, and (8) tumor. (d) Mean afterglow intensity of the organs in panel (c).

Fig. 7 The information readout by ZGO and ZGO–5EDTA at RT and 220 °C.

Application in information storage

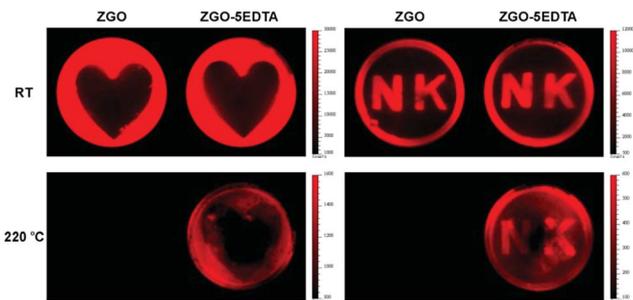We also tested the potential application of ZGO and ZGO–5EDTA in information storage. The information (the heart shape and N K letters) was first restored by the photomask-protected illumination of 254 nm and then, the afterglow was read using a CCD camera. As shown in Fig. 7, both ZGO and ZGO–5EDTA display fine shapes at room temperature, but only ZGO–5EDTA with deep traps has a recognizable readout at a high temperature of 220 °C. These data further support the existence of deep traps in ZGO–5EDTA, and demonstrate that the ZGO–EDTA from EDTA etching has great potential for information storage.

Conclusions

We present a novel and simple EDTA-etching strategy for regulating the traps, size and aqueous-dispersibility of ZGO–EDTA. The EDTA etching ability of the sintered ZGO results in effective reduction in size and great improvement in the aqueous-dispersibility. Moreover, EDTA etching alters the density of mediate traps and generates new deep traps, thus achieving massive production of (ultra)small ZGO–EDTA with fine aqueous-dispersibility and suitable mediate/deep traps. As EDTA can interact with most metals, this simple EDTA etching strategy would be prospectively applied to other PLNPs, and the resultant PLNPs–EDTA would find wide applications in biological field and information storage.

Conflicts of interest

There are no conflicts to declare.

Acknowledgements

Notes and references

1 Y. Li, M. Gecevicius and J. R. Qiu, *Chem. Soc. Rev.*, 2016, **45**, 2090–2136.
2 T. Lecuyer, E. Teston, G. Ramirez-Garcia, T. Maldiney, B. Viana, J. Seguin, N. Mignet, D. Scherman and C. Richard, *Theranostics*, 2016, **6**, 2488–2524.
3 S. K. Singh, *RSC Adv.*, 2014, **4**, 58674–58698.
4 J. Wang, Q. Q. Ma, Y. Q. Wang, H. J. Shen and Q. Yuan, *Nanoscale*, 2017, **9**, 6204–6218.
5 S.-K. Sun, H.-F. Wang and X.-P. Yan, *Acc. Chem. Res.*, 2018, **51**, 1131–1143.
6 L.-J. Chen, S.-K. Sun, Y. Wang, C.-X. Yang, S.-Q. Wu and X.-P. Yan, *ACS Appl. Mater. Interfaces*, 2016, **8**, 32667–32674.
7 Z. Zhou, W. Zheng, J. Kong, Y. Liu, P. Huang, S. Zhou, Z. Chen, J. Shi and X. Chen, *Nanoscale*, 2017, **9**, 6846–6853.
8 B.-Y. Wu, H.-F. Wang, J.-T. Chen and X.-P. Yan, *J. Am. Chem. Soc.*, 2011, **133**, 686–688.
9 B.-Y. Wu and X.-P. Yan, *Chem. Commun.*, 2015, **51**, 3903–3906.
10 N. Li, Y. H. Li, Y. Y. Han, W. Pan, T. T. Zhang and B. Tang, *Anal. Chem.*, 2014, **86**, 3924–3930.
11 A. Abdukayum, J.-T. Chen, Q. Zhao and X.-P. Yan, *J. Am. Chem. Soc.*, 2013, **135**, 14125–14133.
12 Y.-J. Li and X.-P. Yan, *Nanoscale*, 2016, **8**, 14965–14970.
13 Y.-C. Lu, C.-X. Yang and X.-P. Yan, *Nanoscale*, 2015, **7**, 17929–17937.
14 H.-X. Zhao, C.-X. Yang and X.-P. Yan, *Nanoscale*, 2016, **8**, 18987–18994.
15 Z. Pan, Y.-Y. Lu and F. Liu, *Nat. Mater.*, 2012, **11**, 58–63.
16 T. Maldiney, A. Bessiere, J. Seguin, E. Teston, S. K. Sharma, B. Viana, A. J. J. Bos, P. Dorenbos, M. Bessodes, D. Gourier, D. Scherman and C. Richard, *Nat. Mater.*, 2014, **13**, 418–426.
17 A. Abdukayum, C.-X. Yang, Q. Zhao, J.-T. Chen, L.-X. Dong and X.-P. Yan, *Anal. Chem.*, 2014, **86**, 4096–4101.
18 S. Q. Wu, C. W. Chi, C. X. Yang and X. P. Yan, *Anal. Chem.*, 2016, **88**, 4114–4121.
19 Y.-J. Chuang, Z. Zhen, F. Zhang, F. Liu, J. P. Mishra, W. Tang, H. Chen, X. Huang, L. Wang, X. Chen, J. Xie and Z. Pan, *Theranostics*, 2014, **4**, 1112–1122.
20 Z. Xue, X. Li, Y. Li, M. Jiang, G. Ren, H. Liu, S. Zeng and J. Hao, *Nanoscale*, 2017, **9**, 7276–7283.
21 S. K. Sharma, D. Gourier, E. Teston, D. Scherman, C. Richard and B. Viana, *Opt. Mater.*, 2017, **63**, 51–58.
22 F. Liu, W. Z. Yan, Y. J. Chuang, Z. P. Zhen, J. Xie and Z. W. Pan, *Sci. Rep.*, 2013, **3**, 1554.
23 Z. Li, Y. Zhang, X. Wu, X. Wu, R. Maudgal, H. Zhang and G. Han, *Adv. Sci.*, 2015, **2**, 1500001.
24 Y. Li, S. Zhou, Y. Li, K. Sharafudeen, Z. Ma, G. Dong, M. Peng and J. Qiu, *J. Mater. Chem. C*, 2014, **2**, 2657–2663.

25 T. Maldiney, B.-T. Doan, D. Alloyeau, M. Bessodes, D. Scherman and C. Richard, *Adv. Funct. Mater.*, 2015, **25**, 331–338.

26 E. Teston, Y. Lalatonne, D. Elgrabli, G. Autret, L. Motte, F. Gazeau, D. Scherman, O. Clement, C. Richard and T. Maldiney, *Small*, 2015, **11**, 2696–2704.

27 Y. Wang, C.-X. Yang and X.-P. Yan, *Nanoscale*, 2017, **9**, 9049–9055.

28 L. Song, X. H. Lin, X. R. Song, S. Chen, X. F. Chen, J. Li and H. H. Yang, *Nanoscale*, 2017, **9**, 2718–2722.

29 J. Shi, X. Sun, J. Li, H. Man, J. Shen, Y. Yu and H. Zhang, *Biomaterials*, 2015, **37**, 260–270.

30 T. Maldiney, B. Ballet, M. Bessodes, D. Scherman and C. Richard, *Nanoscale*, 2014, **6**, 13970–13976.

31 L.-J. Chen, C.-X. Yang and X.-P. Yan, *Anal. Chem.*, 2017, **89**, 6936–6939.

32 B. Zheng, H.-B. Chen, P.-Q. Zhao, H.-Z. Pan, X.-L. Wu, X.-Q. Gong, H.-J. Wang and J. Chang, *ACS Appl. Mater. Interfaces*, 2016, **8**, 21603–21611.

33 S.-Q. Wu, C.-X. Yang and X.-P. Yan, *Adv. Funct. Mater.*, 2017, **27**, 1604992.

34 R. Abdurahman, C.-X. Yang and X.-P. Yan, *Chem. Commun.*, 2016, **52**, 13303–13306.

35 J. Shi, X. Sun, S. Zheng, J. Li, X. Fu and H. Zhang, *Biomaterials*, 2018, **152**, 15–23.

36 Y.-J. Li, C.-X. Yang and X.-P. Yan, *Anal. Chem.*, 2018, **90**, 4188–4195.

37 Y. Zhuang, Y. Lv, L. Wang, W. Chen, T.-L. Zhou, T. Takeda, N. Hirosaki and R.-J. Xie, *ACS Appl. Mater. Interfaces*, 2018, **10**, 1854–1864.

38 Y. Zhuang, L. Wang, Y. Lv, T.-L. Zhou and R.-J. Xie, *Adv. Funct. Mater.*, 2018, **28**, 1705769.

39 X. Xu, L. Yan, X. Yu, H. Yu, T. Jiang, Q. Jiao and J. Qiu, *Mater. Lett.*, 2013, **99**, 158–160.

40 T. Maldiney, C. Richard, J. Seguin, N. Wattier, M. Bessodes and D. Scherman, *ACS Nano*, 2011, **5**, 854–862.

41 Z. Li, Y. Zhang, X. Wu, L. Huang, D. Li, W. Fan and G. Han, *J. Am. Chem. Soc.*, 2015, **137**, 5304–5307.

42 J. P. Shi, X. Sun, J. F. Zhu, J. L. Li and H. Zhang, *Nanoscale*, 2016, **8**, 9798–9804.

43 B. B. Srivastava, A. Kuang and Y. Mao, *Chem. Commun.*, 2015, **51**, 7372–7375.

44 E. Teston, S. Richard, T. Maldiney, N. Lievre, G. Y. Wang, L. Motte, C. Richard and Y. Lalatonne, *Chem.–Eur. J.*, 2015, **21**, 7350–7354.

45 A. Bessiere, S. K. Sharma, N. Basavaraju, K. R. Priolkar, L. Binet, B. Viana, A. J. J. Bos, T. Maldiney, C. Richard, D. Scherman and D. Gourier, *Chem. Mater.*, 2014, **26**, 1365–1373.

46 S. P. Yeap, *Powder Technol.*, 2018, **323**, 51–59.

47 Y. Yuan, W. Du and X. Qian, *J. Mater. Chem.*, 2012, **22**, 653–659.

48 M. Xing, J. Zhang, F. Chen and B. Tian, *Chem. Commun.*, 2011, **47**, 4947–4949.

49 D. Gourier, A. Bessiere, S. K. Sharma, L. Binet, B. Viana, N. Basavaraju and K. R. Priolkar, *J. Phys. Chem. Solids*, 2014, **75**, 826–837.

50 J. S. Kim, H. I. Kang, W. N. Kim, J. I. Kim, J. C. Choi, H. L. Park, G. C. Kim, T. W. Kim, Y. H. Hwang, S. I. Mho, M. C. Jung and M. Han, *Appl. Phys. Lett.*, 2003, **82**, 2029–2031.

51 J. Su, S. Ye, X. Yi, F. Q. Lu, X. B. Yang and Q. Y. Zhang, *Opt. Mater. Express*, 2017, **7**, 734–743.